Cross-Tracer and Cross-Scanner Transfer Learning-Based Attenuation Correction for Brain SPECT

Hao Sun, Yu Du, Ching-Ni Lin, Han Jiang, Wenbo Huang, Pai-Yi Chiu, Guang-Uei Hung, Lijun Lu, and Greta S. P. Mok, *Senior Member, IEEE*

***Abstract*—This study aims to investigate robust attenuation correction (AC) by generating attenuation maps (μ-maps) from nonattenuation-corrected (NAC) brain SPECT data using transfer learning (TL). Four sets of brain SPECT data (4×30) were retrospectively collected: S-TRODAT-1, S-ECD, G-TRODAT-1, and G-ECD. A 3-D attention-based conditional generative adversarial network was pretrained using 22 paired 3-D NAC SPECT images and corresponding CT μ-maps for four patient groups. Various numbers (n = 4–22) of paired NAC SPECT and corresponding μ-maps from S-TRODAT-1 were then used to fine-tune (FT) the other three pretrained deep learning (DL) networks, i.e., S-ECD, G-TRODAT-1, and G-ECD. All patients in S-TRODAT-1 group were tested on their own network (DL-AC), and on the pretrained models with FT (FT-AC) and without FT (NFT-AC). The FT-AC methods used 22 (FT22), 12 (FT12), 8 (FT8), and 4 (FT4) paired data for FT, respectively. Our results show that FT22 and FT12 could outperform DL-AC for cross-tracer S-ECD and cross-scanner G-TRODAT-1 using CT-based AC (CT-AC) as the reference. FT22 also outperforms DL-AC for cross-tracer+cross-scanner G-ECD. FT8 performs comparably to DL-AC, while FT4 is worse than DL-AC but still better than NAC and NFT-AC in each group. Attenuation map generation is feasible for brain SPECT based on cross-tracer and/or cross-scanner FT-AC using a smaller number of patient data. The FT-AC performance improves as the number of data used for FT increases.**

***Index Terms*—Attenuation correction (AC), brain SPECT, ^{99m}Tc-TRODAT-1, ^{99m}Tc-ECD, transfer learning (TL).**

I. Introduction

THE PREVALENCE of neurodegenerative diseases, such as Parkinson's disease (PD) and Alzheimer's disease (AD), is increasing yearly, posing substantial economic and societal burdens [1]. Early and accurate diagnosis is crucial for the patient management of neurodegenerative diseases. Dopamine transporter (DAT) SPECT has been widely used in the early diagnosis of PD [2], [3], [4] due to its ability to detect nigrostriatal dopaminergic cell neurons accurately [5]. Commonly used radiopharmaceuticals for DAT SPECT include ^{123}I-FP-CIT [6] and ^{99m}Tc-TRODAT-1 [7], while the latter is a more cost-effective approach without the need for a cyclotron. Visual assessment combined with quantification matrices, e.g., specific binding ratio (SBR) and the asymmetry index (ASI) of the left and right striatal uptake, is a standard clinical practice for PD diagnosis [8]. On the other hand, ^{99m}Tc-ECD provides a noninvasive and quantitative measure of regional cerebral blood flow [9], [10]. It has been used for differential diagnosis [11], disease progression monitoring [12], and assessment of treatment efficacy [13] in various neurodegenerative diseases, such as AD. However, photon attenuation limits the quantitative accuracy for tracer uptake in SPECT, and this effect is more pronounced in the center of the field of view. Therefore, attenuation correction (AC) is essential for brain SPECT [14].

CT-based AC (CT-AC) is feasible for brain SPECT when bimodal SPECT-CT is available [15], while it is unavailable for standalone SPECT or dedicated SPECT scanners for organ-specific imaging [16]. Moreover, CT and SPECT registration may be affected by the voluntary and involuntary head movements of neurodegenerative patients [17], [18]. CT radiation may also increase cancer risk [19]. Chang's method [20] was developed for CT-less brain SPECT AC (Chang-AC), assuming homogenous tissue distribution. However, Chang-AC does not consider the substantial attenuation from the skull bone and the head-holder of the scanner, leading to inferior performance as compared to CT-AC. Nutys et al. [21] proposed a maximum-likelihood reconstruction of attenuation and activity (MLAA) method to simultaneously reconstruct tracer activity and attenuation maps (μ-maps) without CT or transmission scan. However, this method is limited by image artifacts and high noise due to crosstalk between the estimated attenuation and activity distribution.

Deep learning (DL) has shown promise for SPECT and PET AC [22], [23]. Two DL-based AC strategies have been used for brain SPECT, including attenuation map generation [24], [25] and attenuation-corrected SPECT image generation [26], [27].

Manuscript received 5 January 2024; revised 26 February 2024; accepted 28 February 2024. Date of publication 8 March 2024; date of current version 3 July 2024. This work was supported in part by the University of Macau under Grant MYRG-CRG 2022-00011-ICMS; in part by the Science and Technology Development Fund of Macau under Grant 0016/2023/RIB1; in part by the National Natural Science Foundation of China under Grant 62371221; in part by the National High-End Foreign Experts Recruitment Plan under Grant G2023030025L; in part by the Guangdong Basic and Applied Basic Research Foundation under Grant 2021A1515011676; and in part by the Science and Technology Program of Guangdong Province under Grant 2022A0505050039. *(Corresponding authors: Guang-Uei Hung; Lijun Lu; Greta S. P. Mok.)*

This work involved human subjects or animals in its research. Approval of all ethical and experimental procedures and protocols was granted by the Local Ethics Approval (SCMH_IRB) under Application No. 1110704.

Please see the Acknowledgment section of this article for the author affiliations.

This article has supplementary material provided by the authors and color versions of one or more figures available at https://doi.org/10.1109/TRPMS.2024.3374207.

Digital Object Identifier 10.1109/TRPMS.2024.3374207

TABLE I
PATIENT DEMOGRAPHICS, SPECT/CT IMAGE ACQUISITION, AND RECONSTRUCTION SETTINGS

	Scanner G		Scanner S	
Hospital	A		B	
Model	GE Infinia Hawkeye		SIEMENS Symbia	
Tracer	^{99m}Tc-TRODAT-1	^{99m}Tc-ECD	^{99m}Tc-TRODAT-1	^{99m}Tc-ECD
Patient Number	30	30	30	30
Age (yr)	71.3±10.3 (range: 49-88)	71.9±15.1 (range: 36-97)	72.2±7.9 (range: 51-84)	70.4±18.1 (range: 27-98)
Gender	19 male/11 female	21 male/9 female	14 male/16 female	19 male/11 female
Injection Activity (MBq)	1110		925	
Acquisition Time (s/view)	60		45	
Collimator Type	low energy high resolution parallel hole			
Primary/ Scatter Window (keV)	126 to 154/114 to 126		126 to 154/109 to 126	
Projection Number	120 over 360°			
Reconstruction	OS-EM, 8 iterations×4 subsets Dual-energy window scatter correction, with or without attenuation correction			
Post-reconstruction Filter	3D Gaussian filter, σ=0.8 voxels		3D Gaussian filter, σ=1.2 voxels	
Matrix/Voxel Size (mm)	64×64×64/4.4181		128×128×128/2.6970	
CT scan	4-slice, 2.5 mAs, 140 kVp, 1.9 pitch, 5 mm thickness		2-slice, 10 mAs, 130 kVp, 1.5 pitch, 3 mm thickness	

Previous studies have shown that using DL to generate attenuation maps is superior to using DL to directly generate attenuation-corrected images in cardiac SPECT [28]. Thus, the former strategy is further investigated in this study. However, standard DL methods usually require a large number of training datasets from the same scanner and tracer. It is particularly challenging for brain SPECT, where clinical data are relatively limited [29]. Transfer learning (TL) has been introduced to alleviate the limited data problem for model training, using a small set of target data for training based on an existing source model. Fine-tuning (FT) is an important strategy in TL that reuses a pretrained model for new related tasks [30]. Chen et al. [31] reported that FT-based AC improved the DL-based AC performance, facilitating the clinical adoption of DL-based AC on new scanners and tracers for myocardial perfusion SPECT. However, the effect of the number of FT data on the performance of FT-based AC methods and the evaluation of different data types for network pretraining are yet to be investigated. The robustness of FT-based AC on brain SPECT also needs further validation.

In this study, we developed a 3-D attention-based conditional generative adversarial network (AttGAN) to estimate μ-maps from nonattenuation-corrected (NAC) SPECT images for brain SPECT using DL-based and FT-based AC strategies. The attention mechanisms effectively capture long-range dependencies in structural information across large regions to enhance interslice and intraslice attention [32]. We demonstrated the feasibility of generating μ-maps for brain SPECT using FT-based AC with a smaller number of cross-tracer and/or cross-scanner patient data as compared to DL-based AC. Qualitative and quantitative assessments for different AC methods were performed using CT-AC SPECT as the reference.

We made notable enhancements in this work compared to our preliminary conference abstract [33].

1) We further optimized the network architecture and loss function to improve the network model performance, leading to enhanced image quality and quantitative accuracy of the generated μ-map and reconstructed SPECT images.
2) We performed additional qualitative and quantitative assessments, particularly for clinical indicators, such as SBR and ASI, which were not evaluated before.
3) Based on a more comprehensive qualitative and quantitative assessment, we revised the conclusions of our preliminary work.

II. MATERIALS AND METHODS

A. Patient Information and Image Acquisition

One hundred and twenty anonymized patients from two affiliated hospitals were retrospectively recruited under local ethics approval (SCMH_IRB No. 1110704). Half of the

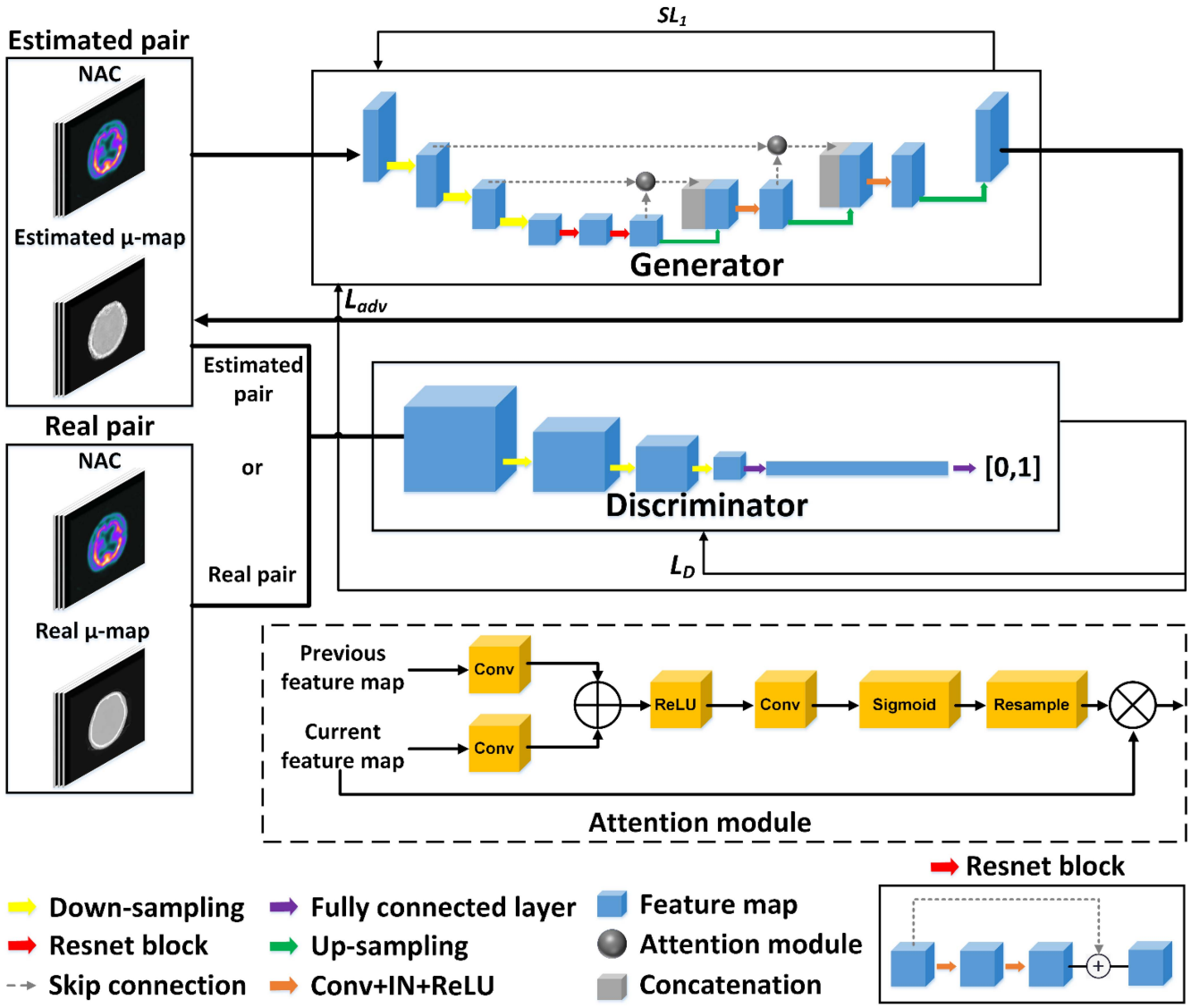

Fig. 1. Schematic of the 3-D AttGAN architecture.

patients ($n = 60$) were injected with 1110 MBq ^{99m}Tc-TRODAT-1, while the other half were injected with the same dosage of ^{99m}Tc-ECD. For each tracer group, half of the patients ($n = 30$) were imaged with scanner G (Infinia, GE HealthCare, USA), while half of them were imaged with scanner S (Symbia, Siemens Healthineers, Germany). Thus, there were a total of four groups of data: S-TRODAT-1, S-ECD , G-TRODAT-1, and G-ECD. Patient demographics and acquisition protocols of the two scanners are shown in Table I. For each scanner, low-dose CT was acquired after the SPECT scan and converted to the attenuation map using a bilinear model [34]. SPECT projections were reconstructed using the ordered subset expectation maximization (OS-EM) algorithm, followed by a 3-D Gaussian post-reconstruction smoothing with or without CT-AC. The attenuation map was registered to the corresponding SPECT data with no mismatches observed.

B. Image Preprocessing

All image data were resampled to a matrix size of $128\times128\times128$ with a voxel size of $2.697\times2.697\times2.697$ mm^3, the same as the scanner S default settings for the subsequent network training. The voxel values of all NAC SPECT images were normalized to [0, 0.1] to match the image intensity range of μ-maps. Subsequently, paired 3-D NAC SPECT images and μ-maps were multiplied by an empirical value of 100 to stabilize the network training [35]. Four kinds of data augmentation were performed for all training data using the Augmentor3D package (https://github.com/amogh3892/Augmentor3D), including rotation with 10°, horizontal flipping, translation with (5, 5, 0) voxels, and shearing with (0.05, 0.05) magnitude.

C. Network Architectures

Inspired by [36], we implemented a 3-D AttGAN, which includes a discriminator D and a generator G, as shown in Fig. 1. The generator loss L_G and the discriminator loss L_D are defined as follows:

$$L_G(x, y) = L_{\text{adv}}(x) + \lambda SL_1(G(x), y) \tag{1}$$

$$L_D(x, y) = \frac{1}{2}((D(x, y) - T_{\text{real}})^2 + (D(x, G(x)) - T_{\text{synthetic}})^2) \tag{2}$$

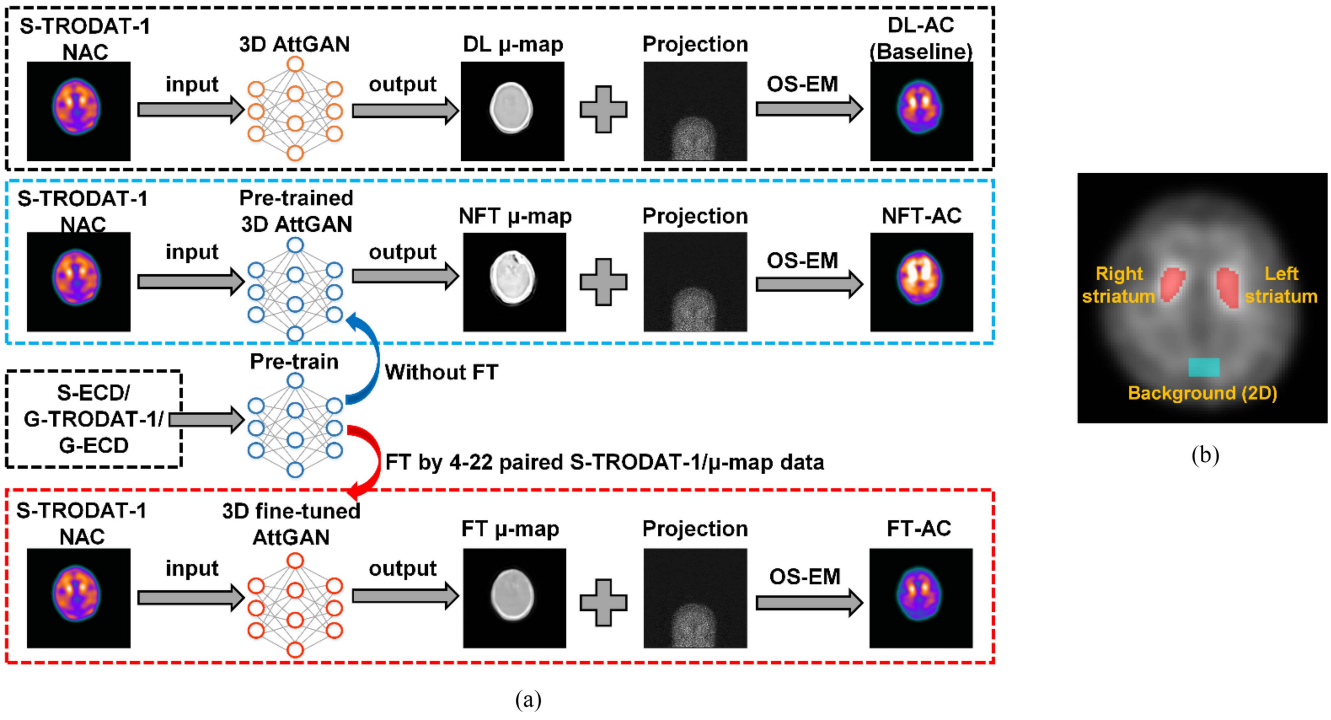

Fig. 2. Schematic of (a) DL-AC, NFT-AC, and FT-AC methods, and (b) striatum ROIs (red mask) and background (blue mask) used in this study.

where x is the NAC SPECT image, and y is the target μ-map. L_{adv} is the adversarial loss function of the generator, SL_1 is the smooth L_1 loss function, which combines the advantages of L_1 and L_2 loss [37]. L_{adv} and SL_1 are defined as

$$L_{\text{adv}}(x) = \frac{1}{2}(D(x, G(x)) - T_{\text{real}})^2 \tag{3}$$

$$SL_1(x, y) = \begin{cases} 0.5(y - G(x))^2, & |y - G(x)| < 1 \\ |y - G(x)| - 0.5, & \text{otherwise} \end{cases} \tag{4}$$

where $T_{\text{real}} = 1$ and $T_{\text{synthetic}} = 0$ are labels for the discriminant results of real and synthetic images, respectively. λ is the weight for SL_1 loss and is set to 10 in this study [38]. We implemented the 3-D AttGAN using Pytorch on a Linux workstation with an NVIDIA RTX A6000 GPU (48 GB). The generator G in this work consisted of a 3-D U-net with three encoder–decoder layers and a Resnet with two blocks. The encoder and decoder consisted of three layers with 3×3×3 convolutional kernels, each followed by an instance normalization (IN) layer and a rectified linear unit (ReLU) activation function. A convolution layer with a stride of 2 and 3×3×3 kernels was used for downsampling. The number of feature channels was doubled in each downsampling step. A nearest neighbor interpolation was used for each upsampling step, followed by a convolutional layer with 3×3×3 kernels, and the number of feature channels was halved. Attention modules were incorporated along with skip connections between the output of the 2nd and 3rd layers in the encoder and the corresponding layers in the decoder. The residual blocks were used to extract the deep features after two downsampling steps with a 0.5 dropout ratio. The discriminator was a convolutional neural network (CNN) architecture consisting of four convolutional layers, a fully connected layer and a sigmoid layer. The first convolution layer of the discriminator consisted of 64 3×3×3 kernel convolutions with a stride of 2, followed by the leaky ReLU (LReLU) function. The 2nd to 4th convolutional layers consisted of 3×3×3 kernel convolutions with a stride of 2, followed by a batch normalization (BN) layer and the LReLU function. The slope of the LReLU function is 0.2. The number of convolution kernels in the following layers was twice that of the previous convolution layers.

D. Network Training

The 3-D AttGAN was pretrained by 22 paired 3-D NAC SPECT images and corresponding μ-maps for each of the four datasets, respectively. The pretrained network using paired S-TRODAT-1 data served as the baseline (DL-AC) and was tested by fivefold cross-validation in this study. NAC SPECT images and corresponding μ-maps from 22, 2, and 6 patients were used for training, validation, and testing the network in each fold. Various numbers (n = 4–22) of paired NAC SPECT and corresponding μ-maps from S-TRODAT-1 were then used to FT the other three pretrained DL networks, i.e., S-ECD, G-TRODAT-1, and G-ECD. All patients in the S-TRODAT-1 dataset were tested on the FT networks (FT-AC) as well as on pretrained networks without FT (NFT-AC) from cross-validations. The FT-AC methods used 22 (FT22), 12 (FT12), 8 (FT8), and 4 (FT4) paired data for FT, respectively. FT22 was tested using fivefold cross-validation, with 2 and 6 patient datasets in each fold used for validation and testing, respectively. FT12, FT8, and FT4 were tested using twofold cross-validation, where two patient datasets were used for validation, and the remaining patient datasets were used for testing in each fold. S-TRODAT-1 projections

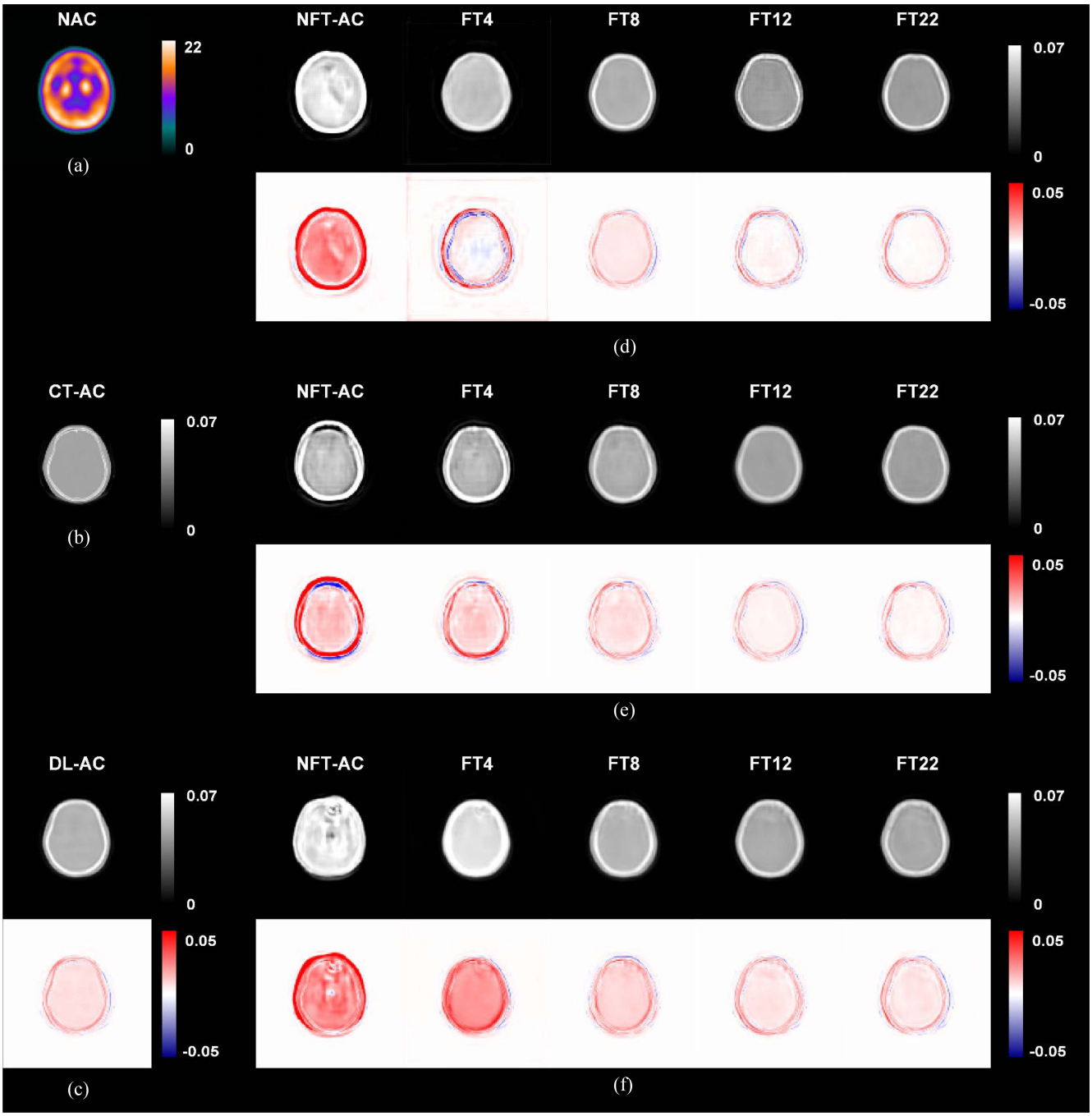

Fig. 3. Representative results of an 80-year-old female patient. Sample axial (a) NAC SPECT image and μ-maps images of (b) CT-AC, (c) DL-AC, NFT-AC, and FT-AC methods with different numbers of FT data for the tested S-TRODAT-1 data using (d) S-ECD (cross-tracer), (e) G-TRODAT-1 (cross-scanner), and (f) G-ECD (cross-tracer+cross-scanner) as the pretrained network. The corresponding error map as compared to CT-AC is shown under each DL-generated μ-map image, respectively.

were then reconstructed with the μ-maps generated from different networks. Fig. 2(a) shows the schematic of DL-AC, NFT-AC and FT-AC. All network models were trained for 500 epochs with a mini-batch of two images. An adaptive learning rate with an initial value of 0.0001 was used for DL-AC and FT-AC.

We performed an ablation study to evaluate the effectiveness of the use of attention modules. DL-AC, NFT-AC, and FT-AC were implemented using a 3-D AttGAN and a standard 3-D conditional generative adversarial network without attention modules (cGAN). The NFT-AC and FT-AC were evaluated using G-TRODAT-1 as the pretrained model.

E. Evaluation Metrics

For voxel-based analysis, normalized mean-square error (NMSE) and structural similarity index (SSIM) were quantified on different methods using CT-AC as the reference

$$\text{NMSE} = \sum_{i=1}^{N} (x(i) - y(i))^2 / \sum_{i=1}^{N} (y(i))^2 \tag{5}$$

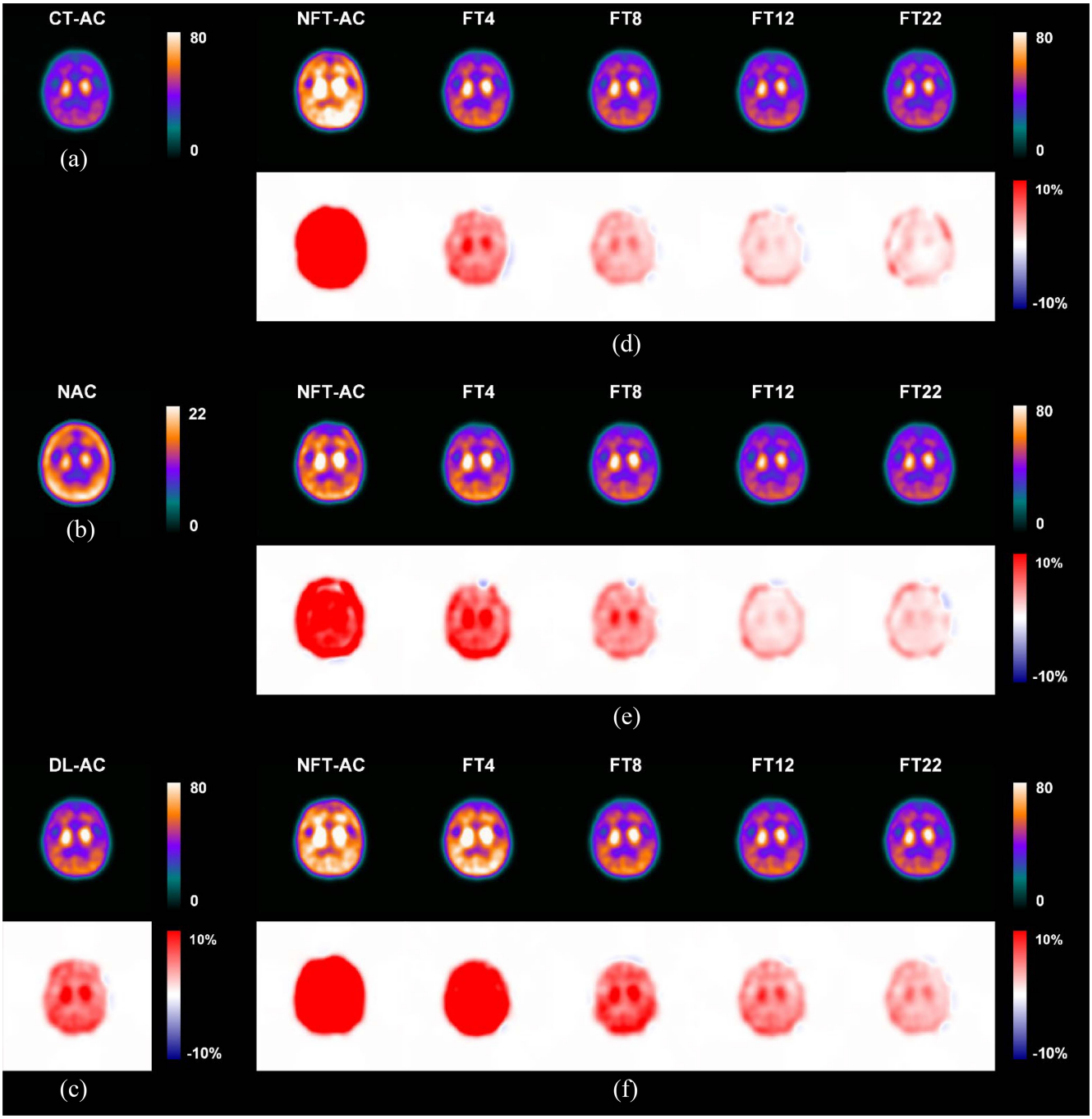

Fig. 4. Representative results of an 80-year-old female patient. Sample axial SPECT images of (a) CT-AC, (b) NAC, (c) DL-AC, NFT-AC, and FT-AC methods with different numbers of FT data for the tested S-TRODAT-1 data using (d) S-ECD (cross-tracer), (e) G-TRODAT-1 (cross-scanner), and (f) G-ECD (cross-tracer+cross-scanner) as the pretrained network. The corresponding error map as compared to CT-AC is shown under each SPECT image, respectively.

$$\text{SSIM} = \frac{(2\mu_x\mu_y + C_1)(2\sigma_{xy} + C_2)}{(\mu_x^2 + \mu_y^2 + C_1)(\sigma_x^2 + \sigma_y^2 + C_2)} \tag{6}$$

where x indicates the predicted image, y indicates the reference image, N indicates the total number of voxels, whereas i is the voxel index. μ_x and μ_y denote the mean value of the predicted image and the reference image. σ_x^2 and σ_y^2 are the variances of the predicted image and the reference image, whereas σ_{xy} indicates their covariance. The parameters $C_1 = (k_1 I)^2$ and $C_2 = (k_2 I)^2$ with constants $k_1 = 0.01$ and $k_2 = 0.03$ were used in this work [39], and I represents the maximum intensity of the reference image. A paired t-test with Bonferroni correction was used to evaluate the NMSE and SSIM results for different AC methods. A p-value <0.05 indicates a significant difference. All statistical analyses were performed using IBM SPSS Statistics 26 software (IBM Corporation, Armonk, NY, USA).

The 3-D left and right striatum and 2-D background masks [Fig. 2(b)] were manually drawn on SPECT images of different AC methods by a nuclear medicine physician

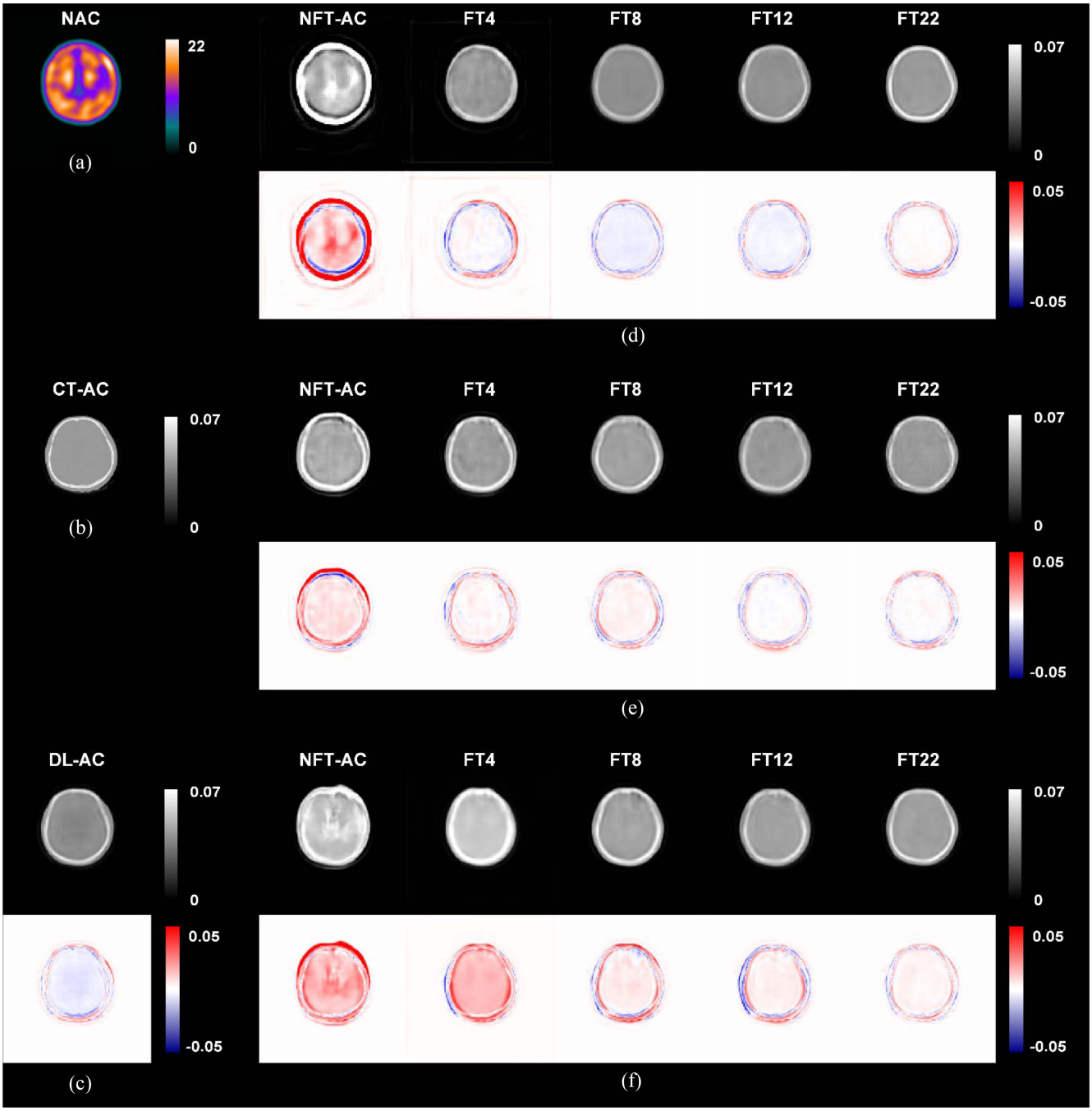

Fig. 5. Representative results of an 81-year-old male patient. Sample axial (a) NAC SPECT image and μ-maps images of (b) CT-AC, (c) DL-AC, NFT-AC, and FT-AC methods with different numbers of FT data for the tested S-TRODAT-1 data using (d) S-ECD (cross-tracer), (e) G-TRODAT-1 (cross-scanner), and (f) G-ECD (cross-tracer+cross-scanner) as the pretrained network. The corresponding error map as compared to CT-AC is shown under each DL-generated μ-map image, respectively.

with ten years of experience. The size of 2-D background mask (10 pixels $\times$ 6 pixels) was chosen for in the cerebellum region, excluding ventricular regions. SBR of the whole striatum to the background region, and ASI of the left and right striatal uptake were evaluated for different AC methods using CT-AC as the reference

$$\text{SBR} = \frac{\text{Mean}_{\text{str}} - \text{Mean}_{\text{bg}}}{\text{Mean}_{\text{bg}}} \tag{7}$$

$$\text{ASI} = \left| \frac{\text{SBR}_{\text{left}} - \text{SBR}_{\text{right}}}{\text{SBR}_{\text{left}} + \text{SBR}_{\text{right}}} \right| \times 100\% \tag{8}$$

where Mean_{str} is the mean count of the striatum and Mean_{bg} is the mean count of the background region. SBR_{left} is the SBR value of left striatum while $\text{SBR}_{\text{right}}$ is the SBR value of right striatum. Bland–Altman plots were applied on SBR and ASI results to evaluate the difference of different AC methods as compared to CT-AC.

TABLE II
NMSE AND SSIM RESULTS (MEAN±SD) OF WHOLE BRAIN SPECT IMAGES FOR DIFFERENT METHODS

Pre-trained Model	AC Method	NMSE (%)	P-value*	SSIM	P-value*
S-TRODAT-1	NAC	41.30±2.83	<0.001	0.6415±0.0676	<0.001
	DL-AC	1.79±1.41	N/A	0.9782±0.0120	N/A
S-ECD	NFT-AC	31.65±28.47	<0.001	0.8321±0.0505	<0.001
	FT22	0.98±0.78	0.005	0.9844±0.0068	0.002
	FT12	1.37±1.12	0.083†	0.9810±0.0080	0.058†
	FT8	2.10±2.92	0.535†	0.9786±0.0076	0.810†
	FT4	2.44±1.77	0.034	0.9718±0.0132	0.002
G-TRODAT-1	NFT-AC	9.93±8.77	<0.001	0.9334±0.0219	<0.001
	FT22	1.03±0.82	0.002	0.9841±0.0064	0.001
	FT12	1.13±0.77	0.012	0.9835±0.0094	<0.001
	FT8	1.39±1.08	0.149†	0.9807±0.0089	0.102†
	FT4	2.29±1.65	0.045	0.9746±0.0102	0.007
G-ECD	NFT-AC	17.27±15.83	<0.001	0.9150±0.0230	<0.001
	FT22	1.09±0.65	0.002	0.9836±0.0074	0.001
	FT12	1.85±2.76	0.898†	0.9787±0.0096	0.701†
	FT8	2.26±2.00	0.094†	0.9748±0.0160	0.089†
	FT4	5.06±5.22	0.001	0.9610±0.0233	<0.001

* Paired *t*-test between DL-AC and other methods with Bonferroni correction. †This indicates that the results of the corresponding method showed no significant differences compared to those of DL-AC.

III. RESULTS

Figs. 3–6 show the sample results of generated μ-maps and SPECT images of CT-AC, NAC, DL-AC, NFT-AC, and FT-AC methods of testing S-TRODAT-1 data. The NFT-AC and FT-AC models were based on S-ECD (cross-tracer), G-TRODAT-1 (cross-scanner), and G-ECD (cross-tracer+cross-scanner) as the pretrained models. The corresponding error maps are estimated using CT-AC μ-maps and SPECT images as references. DL-AC and all FT-AC methods show improved image quality as compared to NAC and NFT-AC. FT22 shows the best performance for the two sample patients. NFT-AC overestimates the μ-maps and SPECT image values for each patient. Increasing the number of FT data improves FT-AC performance.

Table II provides the detailed NMSE and SSIM results of whole brain SPECT images of different methods across all patients in the tested S-TRODAT-1 dataset, and the results are consistent with visual image results. FT22 shows the best performance in each group. The NMSE and SSIM of FT22 of each group are significantly better than DL-AC (p <0.05). For cross-scanner G-TRODAT-1, the NMSE and SSIM of FT12 are significantly better than DL-AC (p <0.05). FT8 is also better than DL-AC but without significant difference (p >0.05). For cross-tracer S-ECD, the NMSE and SSIM of FT12 are better than DL-AC but without significant difference (p >0.05). FT8 is worse than DL-AC without significant difference (p >0.05). For cross-tracer+cross-scanner G-ECD, both FT12 and FT8 yield worse NMSE and SSIM results than DL-AC without significant difference (p >0.05). The NMSE and SSIM of FT4 are significantly worse than DL-AC with statistical significance (p <0.05) in each group. NFT-AC is significantly worse than DL-AC and all FT-AC methods, yet it outperforms NAC in terms of NMSE and SSIM results in each group.

Fig. 7 depicts the joint histogram and linear regression analysis results of different AC methods on whole brain S-TRODAT-1 SPECT images across all tested patients using CT-AC as the reference. DL-AC (slope = 1.0400, R^2 = 0.984) shows a higher correlation with CT-AC than NAC (slope = 0.3667, R^2 = 0.888). For cross-tracer S-ECD and cross-scanner G-TRODAT-1, FT22 and FT12 show better performance than DL-AC, resulting in correlation coefficients of (slope = 1.0281, R^2 = 0.990) and (slope = 1.0169, R^2 = 0.987) for cross-tracer S-ECD, (slope = 0.9990, R^2 = 0.990) and (slope = 1.0299, R^2 = 0.989) for cross-scanner G-TRODAT-1, respectively. For cross-tracer+cross-scanner G-ECD, FT22 (slope = 1.0099, R^2 = 0.989) is better than DL-AC while FT12 (slope = 1.0265, R^2 = 0.980) is worse than DL-AC. FT8 and FT4 are worse than DL-AC except for FT8 of cross-scanner G-TRODAT-1, yet all FT results are better than NAC and NFT-AC. NFT-AC shows better performance than NAC in each group.

Fig. 8 shows the Bland–Altman plots of SBR and ASI results of different AC methods across all S-TRODAT-1 patients using CT-AC as the reference. NAC shows lower

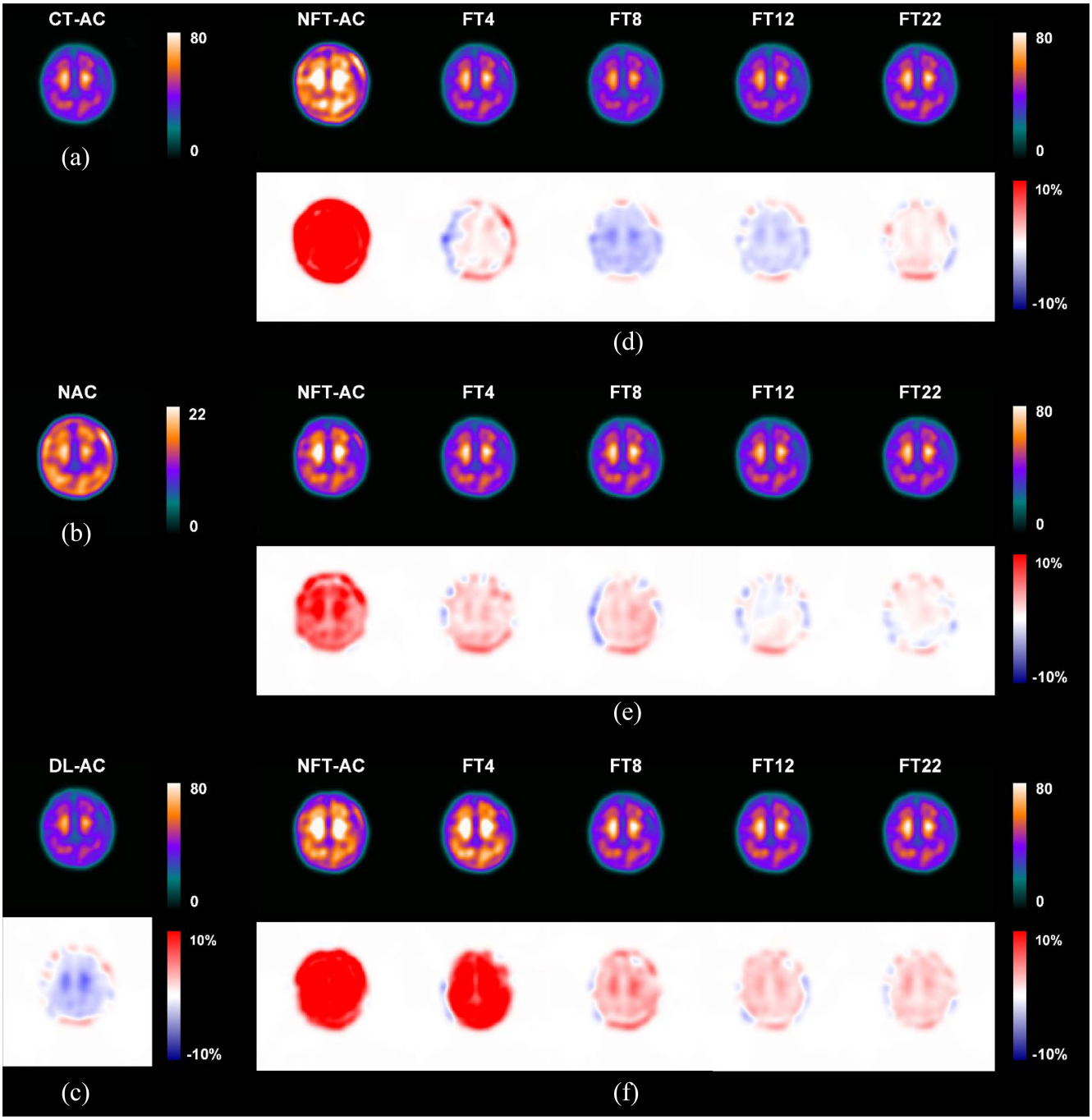

Fig. 6. Representative results of an 81-year-old male patient. Sample axial SPECT images of (a) CT-AC, (b) NAC, (c) DL-AC, NFT-AC, and FT-AC methods with different numbers of FT data for the tested S-TRODAT-1 data using (d) S-ECD (cross-tracer), (e) G-TRODAT-1 (cross-scanner), and (f) G-ECD (cross-tracer+cross-scanner) as the pretrained network. The corresponding error map as compared to CT-AC is shown under each SPECT image, respectively.

SBR values (mean %Difference of −44.86) than CT-AC. DL-AC shows a narrower distribution (mean %Difference of 0.4228) with a smaller 95% confidence interval (CI) of [−8.754, 9.600] than NAC. For cross-tracer S-ECD, FT22 and FT12 show better performance than DL-AC with a smaller 95% CI of [−7.639, 7.333] and [−7.904, 10.18], respectively. For cross-tracer G-TRODAT-1, FT22, FT12 and FT8 outperform DL-AC, showing the 95% CIs of [−5.230, 7.886], [−5.037, 10.32], and [−4.757, 12.04], respectively. For cross-tracer+cross-scanner G-ECD, FT22 outperforms DL-AC with 95% CIs of [−6.825, 8.741], but FT12 is worse than DL-AC with 95% CIs of [−8.588, 11.30]. FT8 of cross-tracer S-ECD and FT8 of cross-tracer+cross-scanner are both worse than DL-AC. FT4 is worse than DL-AC in each group, yet better than NFT-AC. NFT-AC shows worse performance than DL-AC and all FT-AC methods in each pretrained model, but it is better than NAC in each group. Overall, cross-scanner FT-AC shows better performance than cross-tracer FT-AC, while both perform better than cross-tracer+cross-scanner FT-AC in terms of SBR assessments. DL-AC is better

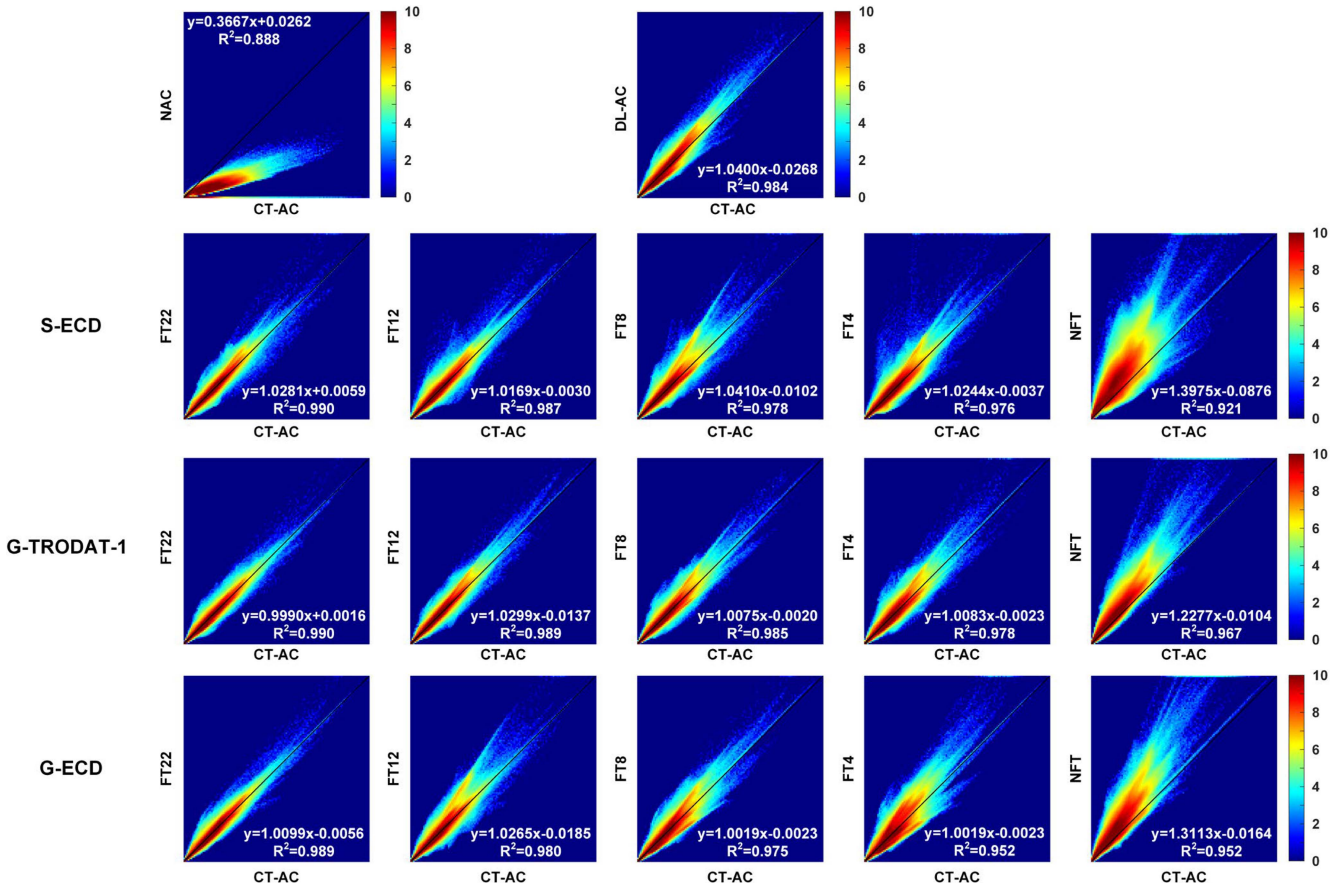

Fig. 7. Joint histogram and linear regression analysis of NAC, DL-AC, different FT-AC, and NFT-AC methods on whole brain S-TRODAT-1 SPECT images across all tested patients using CT-AC as the reference.

than NAC for the ASI results, with a smaller 95% CI of [−3.566, 4.144] versus [−5.505, 10.75]. FT22 shows the best performance in each group. FT22 and FT12 are better than DL-AC with smaller 95% CIs of [−2.711, 3.289] and [−2.985, 3.896] for cross-tracer S-ECD, as well as [−2.740, 3.208] and [−2.960, 3.362] for cross-scanner G-TRODAT-1, respectively. For cross-tracer+cross-scanner G-ECD, FT22 is also better than DL-AC with a smaller 95% CI of [−3.315, 3.693]. FT8 (95% CI of [−2.925, 3.800] and FT4 (95% CI of [−4.024, 3.053] outperform DL-AC in cross-scanner G-TRODAT-1. While for cross-tracer S-ECD and cross-tracer+cross-scanner G-ECD, FT8 and FT4 are both worse than DL-AC. NFT-AC performs worse than DL-AC and all FT-AC in each pretrained model, yet better than NAC for cross-scanner G-TRODAT-1 and cross-tracer+cross-scanner G-ECD. For the ASI assessments, cross-scanner FT-AC outperforms cross-tracer FT-AC, while both are superior to cross-tracer+cross-scanner FT-AC.

In terms of the effectiveness of attention modules, the ablation study demonstrates that AttGAN outperforms cGAN for brain SPECT AC (Table S1 and Fig. S1 in the supplementary data).

IV. Discussion

This work demonstrates the feasibility of attenuation map generation for brain SPECT based on cross-tracer and/or cross-scanner FT-AC using a smaller number of specific patient data for FT as compared to DL-AC. FT-AC performance improves as the number of data used for FT increases. FT-AC can perform accurate AC and even outperform DL-AC for brain SPECT when the number of FT data is $\geq$8 in this study. Additionally, all FT-AC outperform NFT-AC, showing the effectiveness of the FT strategy. Cross-scanner FT-AC is better than cross-tracer FT-AC, while both are better than cross-tracer+cross-scanner FT-AC.

DL-AC approaches usually require a large number of datasets from the same scanner and tracer to generate robust models, which may not be applicable for real clinical implementation due to the availability of limited datasets [40], [41]. Determining an exact threshold of data sufficiency for DL-AC models tailored to specific tracers or scanners or DL-models for other applications remains challenging in general. However, by closely monitoring the convergence of training and validation losses and ensuring that the generated images meet clinical diagnostic requirements [26], [28], we can generally infer that the quantity of data employed for training the AC model ($n = 30$ in this study) is sufficient. Compared to DL-AC, FT-AC reuses a pretrained DL-AC model from other existing data instead of starting the training from scratch. FT12 and FT8 could achieve comparable or better performance than DL-AC, proving the potential for generalizable brain SPECT μ-maps generation without the need to collect a large number of specific data and retraining

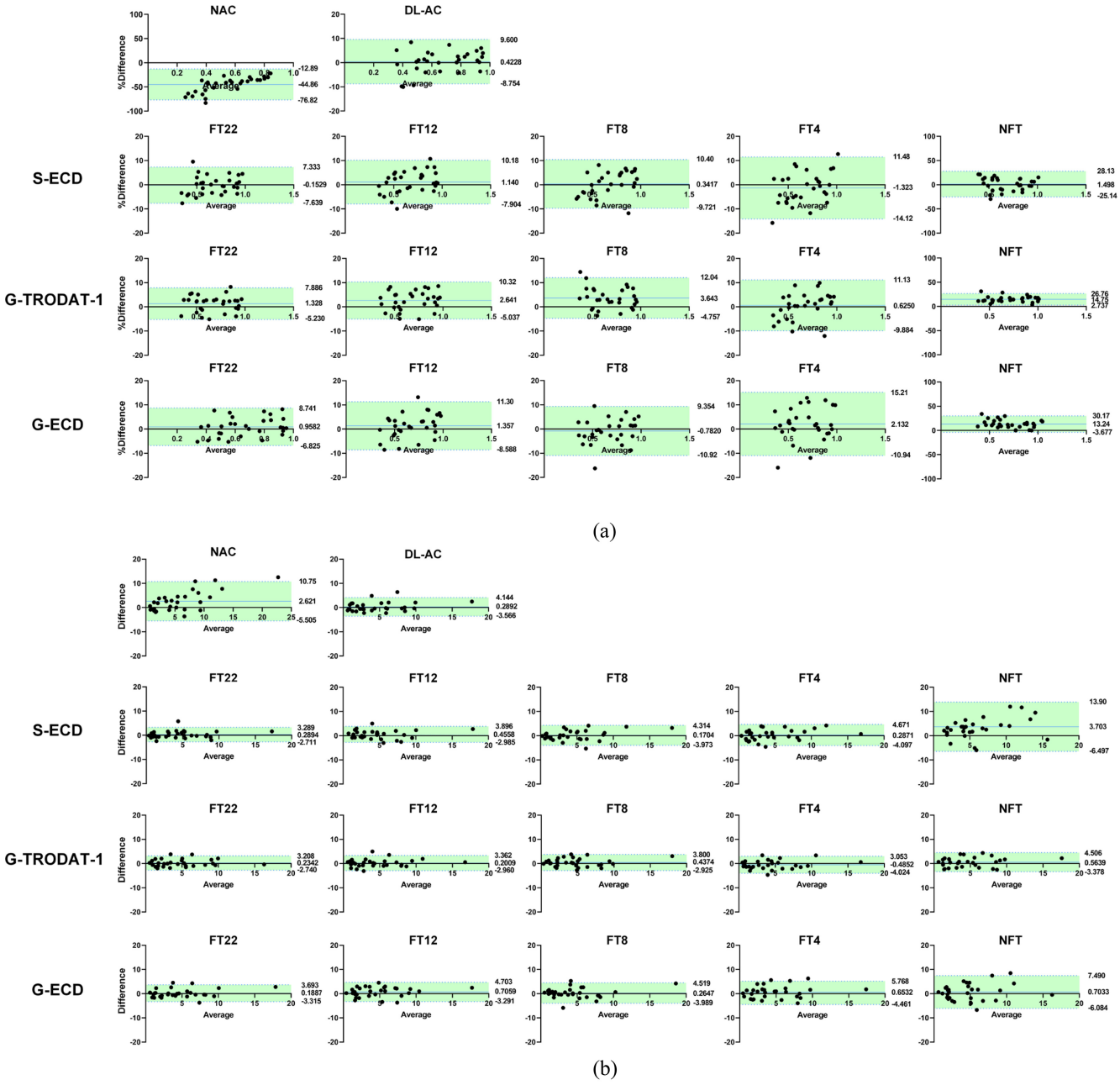

Fig. 8. Bland–Altman plots of (a) SBR and (b) ASI results of NAC, DL-AC, different FT-AC, and NFT-AC methods across all patients in the S-TRODAT-1 dataset using CT-AC as the reference.

on new networks. Unlike the conventional FT method that uses a small amount of data, FT22 uses the same amount of data for FT as compared to the baseline DL-AC and further improves DL-AC performance. This may indicate that instead of directly mixing different data types to increase the sample size for ensemble training, with inferior results observed in our previous study [42], the use of FT strategies could be more promising to improve the model generalizability.

Our experimental results show that AC for ^{99m}Tc-TRODAT-1 brain SPECT would be essential for diagnostic purposes as it is difficult to distinguish between the striatum and background regions in NAC SPECT images. AC is also essential for absolute quantification of ^{99m}Tc-TRODAT-1 brain SPECT [43] as NAC significantly underestimates SBRs by a mean of 44.86% and shows [−5.505%, 10.75%] ASI difference as compared to the reference CT-AC. Compared with NAC, FT-AC and DL-AC can better differentiate the striatum and background regions on SPECT images with closer SBR and ASI results to the reference CT-AC. FT-AC shows better performance than DL-AC for visual images and SBR and ASI assessments when the number of FT data is sufficient.

In terms of various qualitative and quantitative assessments, cross-scanner FT-AC shows better performance than cross-tracer FT-AC, yet both outperform cross-tracer+cross-scanner FT-AC. Generally, the closer the pretraining data are to the test data, the better the pretrained network model performs.

Though the image acquisition and reconstruction settings of S-TRODAT-1 differ from G-TRODAT-1, the image features of S-TRODAT-1 were still similar to G-TRODAT-1. Moreover, we implemented the resampling step to make the matrix size and voxel size consistent for the two scanners, which should mitigate the differences between data acquired from different scanners. As expected, cross-tracer+cross-scanner FT-AC performs relatively inferior as compared to the other two pretrained models, given that G-ECD data may deviate more from S-TRODAT-1 compared to S-ECD and G-TRODAT-1.

Compared to our previous work [44], this work estimates μ-maps from NAC PET images instead of directly estimating CT-AC images for better DL-AC performance [28]. We have further optimized our network architecture for our targeted application, including the use of attention modules, enhanced loss function (smooth L1 instead of L1), an additional downsampling and upsampling layer, and reduced ResNet blocks. This work also explores the performance of the use of different numbers of FT data and investigates a different application on cross-tracer, cross-scanner, and cross-tracer+cross-scanner brain SPECT datasets.

One limitation of FT-AC is the need for sufficient pretraining data. The inadequately pretrained networks may propagate errors to the FT network model, causing image artifacts [45]. TL based on simulation data may be an effective solution in the case of insufficient pretraining data [46]. Besides, Guo et al. [47] proposed to integrate domain knowledge in DL for CT-free PET imaging, achieving efficient and robust performance of attenuation and scatter correction on cross-scanner or cross-tracer PET data. Federated learning has shown great potential for multi-institutional PET attenuation and scatter correction [48], which could be adopted for cross-tracer and/or cross-scanner SPECT data.

Another limitation of this study is that the number of data used for FT may not be generalizable to other TL tasks in SPECT AC. In our study, all NMSE and SSIM results of FT8 and FT12 showed no statistically significant differences compared to DL-AC. This suggests that when the amount of target domain data exceeds 36% of the large-scale target domain data, the target domain SPECT AC model obtained through TL can achieve performance comparable to a model trained with large-scale target domain data. However, Chen et al. [31] found that even with FT data (ten studies) accounting for 1/7 of the test data (70 studies), the resulting network model was also considered acceptable. The effectiveness of TL could be influenced by the differences between the source and target domains. Hence, determining the required amount of target domain data for TL in a specific tracer or scanner could be task-dependent and needs further evaluation. The datasets used in this work are still relatively small, though a fivefold data augmentation technique is implemented. However, it also represents the need for TL in cross-scanner and cross-tracer data for brain SPECT, which is an application lacking a large number of patient datasets. More patient cohorts from different centers are warranted for further evaluation. More effective network architectures are also warranted.

V. Conclusion

In this study, we demonstrate the feasibility of attenuation map generation for brain SPECT based on cross-tracer and/or cross-scanner FT-AC. Qualitative and quantitative results show that FT-AC could even outperform DL-AC for brain SPECT, showing a great value for the use of general brain SPECT data for TL-based AC. We also observe that cross-scanner FT-AC outperforms cross-tracer FT-AC, which both outperform cross-tracer+cross-scanner FT-AC.

Acknowledgment

All authors declare that they have no known conflicts of interest in terms of competing financial interests or personal relationships that could have an influence or are relevant to the work reported in this article.

Hao Sun is with the Biomedical Imaging Laboratory (BIG), Department of Electrical and Computer Engineering, Faculty of Science and Technology, University of Macau, Macau, SAR, China, and also with the School of Biomedical Engineering, Southern Medical University, Guangzhou 510515, China.

Yu Du and Greta S. P. Mok are with the Biomedical Imaging Laboratory (BIG), Department of Electrical and Computer Engineering, Faculty of Science and Technology, and the Center for Cognitive and Brain Sciences, Institute of Collaborative Innovation, University of Macau, Macau, SAR, China (e-mail: gretamok@um.edu.mo).

Ching-Ni Lin is with the Department of Nuclear Medicine, Show Chwan Memorial Hospital, Changhua County 500, Taiwan.

Wenbo Huang is with the Biomedical Imaging Laboratory (BIG), Department of Electrical and Computer Engineering, Faculty of Science and Technology, University of Macau, Macau, SAR, China.

Han Jiang is with the Biomedical Imaging Laboratory (BIG), Department of Electrical and Computer Engineering, Faculty of Science and Technology, University of Macau, Macau, SAR, China, and also with the PET-CT Center, Fujian Medical University Union Hospital, Fuzhou 350001, China.

Pai-Yi Chiu is with the Department of Neurology, Show Chwan Memorial Hospital, Changhua County 500, Taiwan.

Guang-Uei Hung is with the Department of Nuclear Medicine, Chang Bing Show Chwan Memorial Hospital, Lukang 505, Taiwan (e-mail: 106143@gmail.com).

Lijun Lu is with the School of Biomedical Engineering, Southern Medical University, Guangzhou 510515, China, also with the Guangdong Provincial Key Laboratory of Medical Image Processing, Southern Medical University, Guangzhou 510515, China, and also with Pazhou Lab, Guangzhou 510330, China (e-mail: ljlubme@gmail.com).

References

[1] M. G. Erkkinen, M.-O. Kim, and M. D. Geschwind, "Clinical neurology and epidemiology of the major neurodegenerative diseases," *Cold. Spring. Harb. Perspect. Biol.*, vol. 10, no. 4, 2018, Art. no. a033118.

[2] G. Fabiani, C. H. F. Camargo, G. S. Froehner, and H. A. G. Teive, "Evaluation of brain SPECT with ^{99m}Tc-TRODAT-1 in the differential diagnosis of parkinsonism," *Park. Disease*, vol. 2022, Mar. 2022, Art. no. 1746540.

[3] V. Gupta, R. Ranjan, R. Verma, E. S. Belho, D. Malik, and H. Mahajan, "Correlation of ^{99m}Tc-TRODAT-11 SPECT imaging findings and clinical staging of Parkinson disease," *Clin. Nucl. Med.*, vol. 44, no. 5, pp. 347–350, 2019.

[4] W. J. Hwang, W. J. Yao, S. P. Wey, and G. Ting, "Reproducibility of 99mTc-TRODAT-1 SPECT measurement of dopamine transporters in Parkinson's disease," *J. Nucl. Med.*, vol. 45, no. 2, pp. 207–213, 2004.

[5] S. R. Suwijn, C. J. Van Boheemen, R. J. De Haan, G. Tissingh, J. Booij, and R. De Bie, "The diagnostic accuracy of dopamine transporter SPECT imaging to detect nigrostriatal cell loss in patients with Parkinson's disease or clinically uncertain parkinsonism: A systematic review," *EJNMMI Res.*, vol. 5, no. 1, pp. 1–8, 2015.

[6] J. Booij et al., "[123I]FP-CIT SPECT shows a pronounced decline of striatal dopamine transporter labelling in early and advanced Parkinson's disease," *J. Neurol. Neurosurg. Psychiatry*, vol. 62, no. 2, pp. 133–40, Feb, 1997.

[7] H. F. Kung, H.-J. Kim, M.-P. Kung, S. K. Meegalla, K. Plössl, and H.-K. Lee, "Imaging of dopamine transporters in humans with technetium-99m TRODAT-1," *Eur. J. Nucl. Med.*, vol. 23, no. 11, pp. 1527–1530, 1996.

[8] N. L. Albert et al., "Implementation of the European multicentre database of healthy controls for [123I] FP-CIT SPECT increases diagnostic accuracy in patients with clinically uncertain parkinsonian syndromes," *Eur. J. Nucl. Med. Mol. Imag.*, vol. 43, pp. 1315–1322, Jul. 2016.

[9] C. Chang, Y. Shiau, J. Wang, S. Ho, and A. Kao, "Abnormal regional cerebral blood flow on 99mTc ECD brain SPECT in patients with primary Sjögren's syndrome and normal findings on brain magnetic resonance imaging," *Ann. Rheum. Dis.*, vol. 61, no. 9, pp. 774–778, 2002.

[10] F. Tanaka, D. Vines, T. Tsuchida, M. Freedman, and M. Ichise, "Normal patterns on 99mTc-ECD brain SPECT scans in adults," *J. Nucl. Med.*, vol. 41, no. 9, pp. 1456–1464, 2000.

[11] K. Van Laere, P. Santens, T. Bosman, J. De Reuck, L. Mortelmans, and R. Dierckx, "Statistical parametric mapping of (99mTc)-ECD SPECT in idiopathic Parkinson's disease and multiple system atrophy with predominant parkinsonian features: Correlation with clinical parameters," *J. Nucl. Med.*, vol. 45, no. 6, pp. 933–942, 2004.

[12] B. Borroniet al., "Combined 99mTc-ECD SPECT and neuropsychological studies in MCI for the assessment of conversion to AD," *Neurobiol. Aging*, vol. 27, no. 1, pp. 24–31, 2006.

[13] C. Usui et al., "Improvements in both psychosis and motor signs in Parkinson's disease, and changes in regional cerebral blood flow after electroconvulsive therapy," *Prog. Neuropsychopharmacol. Biol. Psychiatry*, vol. 35, no. 7, pp. 1704–1708, 2011.

[14] N. Rajeevan, I. G. Zubal, S. Q. Ramsby, S. S. Zoghbi, J. Seibyl, and R. B. Innis, "Significance of nonuniform attenuation correction in quantitative brain SPECT imaging," *J. Nucl. Med.*, vol. 39, no. 10, pp. 1719–1726, 1998.

[15] G. Mariani et al., "A review on the clinical uses of SPECT/CT," *Eur. J. Nucl. Med. and Mol. Imaging*, vol. 37, no. 10, pp. 1959–1985, 2010.

[16] M. Stam, E. Verwer, J. Booij, S. Adriaanse, C. de Bruin, and T. de Wit, "Performance evaluation of a novel brain-dedicated SPECT system," *EJNMMI Phys.*, vol. 5, pp. 1–14, Mar. 2018.

[17] D. Zhang, B.-H. Yang, N. Y. Wu, and G. S. P. Mok, "Respiratory average CT for attenuation correction in myocardial perfusion SPECT/CT," *Ann. Nucl. Med.*, vol. 31, pp. 172–180, Feb. 2017.

[18] Y. Lyu, G. Chen, Z. Lu, Y. Chen, and G. S. Mok, "The effects of mismatch between SPECT and CT images on quantitative activity estimation—A simulation study," *Z. Med. Phys.*, vol. 33, no. 1, pp. 54–69, 2023.

[19] I. Rausch, F. G. Füchsel, C. Kuderer, M. Hentschel, and T. Beyer, "Radiation exposure levels of routine SPECT/CT imaging protocols," *Eur. J. Radiol.*, vol. 85, no. 9, pp. 1627–1636, 2016.

[20] L.-T. Chang, "A method for attenuation correction in radionuclide computed tomography," *IEEE. Trans. Nucl. Sci.*, vol. 25, no. 1, pp. 638–643, 1978.

[21] J. Nuyts, P. Dupont, S. Stroobants, R. Benninck, L. Mortelmans, and P. Suetens, "Simultaneous maximum a posteriori reconstruction of attenuation and activity distributions from emission sinograms," *IEEE Trans. Med. Imag.*, vol. 18, no. 5, pp. 393–403, May 1999.

[22] J. S. Lee, "A review of deep-learning-based approaches for attenuation correction in positron emission tomography," *IEEE Trans. Radiat. Plasma Med. Sci.*, vol. 5, no. 2, pp. 160–184, Mar. 2021.

[23] X. Chen, and C. Liu, "Deep-learning-based methods of attenuation correction for SPECT and PET," *J. Nucl. Cardiol.*, vol. 30, no. 5, pp. 1859–1878, 2023.

[24] Y. Chen, M. C. Goorden, and F. J. Beekman, "Convolutional neural network based attenuation correction for 123I-FP-CIT SPECT with focused striatum imaging," *Phys. Med. Biol.*, vol. 66, no. 19, 2021, Art. no. 195007.

[25] Y. Chen, M. C. Goorden, and F. J. Beekman, "Automatic attenuation map estimation from SPECT data only for brain perfusion scans using convolutional neural networks," *Phys. Med. Biol.*, vol. 66, no. 6, 2021, Art. no. 065006.

[26] K. Sakaguchi, H. Kaida, S. Yoshida, and K. Ishii, "Attenuation correction using deep learning for brain perfusion SPECT images," *Ann. Nucl. Med.*, vol. 35, no. 5, pp. 589–599, 2021.

[27] T. Murata et al., "Development of attenuation correction methods using deep learning in brain-perfusion single-photon emission computed tomography," *Med. Phys.*, vol. 48, no. 8, pp. 4177–4190, 2021.

[28] Y. Du et al., "Deep-learning-based estimation of attenuation map improves attenuation correction performance over direct attenuation estimation for myocardial perfusion SPECT," *J. Nucl. Cardiol.*, vol. 30, pp. 1022–1037, Sep. 2022.

[29] S. Tiepolt et al., "Current radiotracers to image neurodegenerative diseases," *EJNMMI Radiopharm. Chem.*, vol. 4, pp. 1–23, Dec. 2019.

[30] K. Weiss, T. M. Khoshgoftaar, and D. Wang, "A survey of transfer learning," *J. Big Data*, vol. 3, no. 1, pp. 1–40, 2016.

[31] X. Chen et al., "Cross-vender, cross-tracer, and cross-protocol deep transfer learning for attenuation map generation of cardiac SPECT," *J. Nucl. Cardiol.*, vol. 29, pp. 3379–3391, 2022.

[32] H. Zhang, I. Goodfellow, D. Metaxas, and A. Odena, "Self-attention generative adversarial networks," 2018, *arXiv:1805.08318*.

[33] H. Sun et al., "Cross-tracer and cross-scanner transfer learning-based attenuation map generation for brain SPECT," *Soc. Nucl. Med.*, vol. 64, no. 1, p. P897, 2023.

[34] J. A. Patton and T. G. Turkington, "SPECT/CT physical principles and attenuation correction," *J. Nucl. Med. Technol.*, vol. 36, no. 1, pp. 1–10, 2008.

[35] I. J. Goodfellow, "NIPS 2016 tutorial: Generative adversarial networks," 2016, *arXiv:1701.00160*.

[36] J. Sun et al., "Fast myocardial perfusion SPECT denoising using an attention-guided generative adversarial network," *Front. Med.*, vol. 10, Feb. 2023, Art. no. 1083413.

[37] R. Girshick, "Fast R-CNN," 2015, *arXiv:1504.08083*.

[38] P. Isola, J.-Y. Zhu, T. Zhou, and A. A. Efros, "Image-to-image translation with conditional adversarial networks," 2017, *arXiv:1611.07004*.

[39] Z. Wang, A. C. Bovik, H. R. Sheikh, and E. P. Simoncelli, "Image quality assessment: from error visibility to structural similarity," *IEEE Trans. Image. Process.*, vol. 13, pp. 600–612, 2004.

[40] N. Rieke et al., "The future of digital health with federated learning," *NPJ Digit. Med.*, vol. 3, no. 1, p. 119, 2020.

[41] C.-R. Shyu et al., "A systematic review of federated learning in the healthcare area: From the perspective of data properties and applications," *Appl. Sci.*, vol. 11, no. 23, 2021, Art. no. 11191.

[42] Y. Du et al., "Generative adversarial network-based attenuation correction for ^{99m}Tc-TRODAT-1 brain SPECT," *Front. Med.*, vol. 10, Aug. 2023, Art. no. 1171118.

[43] N. A. Zainudin, N. Zulkifli, K. Hamid, H. Hashim, and S. Mansor, "Experimental evaluation of absolute quantification in 99mTc-TRODAT-1 SPECT/CT brain dopamine transporter (DAT) studies," *J. Appl. Clin. Med. Phys.*, vol. 23, no. 8, 2022, Art. no. e13723.

[44] H. Sun et al., "Transfer learning-based attenuation correction for static and dynamic cardiac PET using a generative adversarial network," *Eur. J. Nucl. Med. Mol. Imag.*, vol. 50, no. 12, pp. 3630–3646, 2023.

[45] S. Bianco, L. Celona, P. Napoletano, and R. Schettini, "On the use of deep learning for blind image quality assessment," *Signal Image Video Process.*, vol. 12, pp. 355–362, Feb. 2018.

[46] K. Gong, J. Guan, C.-C. Liu, and J. Qi, "PET image denoising using a deep neural network through fine tuning," *IEEE Trans. Radiat. Plasma Med. Sci.*, vol. 3, no. 2, pp. 153–161, Mar. 2019.

[47] R. Guo et al., "Using domain knowledge for robust and generalizable deep learning-based CT-free PET attenuation and scatter correction," *Nat. Commun.*, vol. 13, no. 1, 2022, Art. no. 5882.

[48] I. Shiri et al., "Decentralized collaborative multi-institutional PET attenuation and scatter correction using federated deep learning," *Eur. J. Nucl. Med. Mol. Imag.*, vol. 50, pp. 1034–1050, Dec. 2022.